Desalination and Water Treatment
www.deswater.com

doi: 10.5004/dwt.2023.30121

315 (2023) 150–159
December

Use of an economical cellulose material for dye removal

Wei Li[a], Liya Zhu[a], Chunrui Liu[a], Zitong Zhao[a], Haoran Ma[a], Shiyao Wang[a], Ruyi Zhou[a], Binbin Zhang[b,*], Yingjie Dai[a,*]

[a]*College of Resources and Environment, Northeast Agricultural University, No. 600 Changjiang Road, Xiangfang District, Harbin 150030, China, emails: dai5188@hotmail.com (Y. Dai), weili@neau.edu.cn (W. Li), 3350095189@qq.com (L. Zhu), 2415768395@qq.com (C. Liu), 3201772928@qq.com (Z. Zhao), 844240468@qq.com (H. Ma), wsy20021001@163.com (S. Wang), 1849877363@qq.com (R. Zhou)*

[b]*Key Laboratory of Soybean Biology in Chinese Ministry of Education, Northeast Agricultural University, No. 600 Changjiang Road, Xiangfang District, Harbin 150030, China, email: binbinzhang@neau.edu.cn (B. Zhang)*

Received 26 June 2023; Accepted 6 November 2023

ABSTRACT

The objective of this study was to investigate the performance and applicability of two adsorbents for the removal of two dyes, namely Neutral red (NR) and Malachite green (MG), from aqueous solutions. The adsorbents were okara adsorbent (OA) and modified okara adsorbent (SOA) prepared from biological waste okara through sodium lauryl sulfate treatment. The changes in surface morphology and functional groups of okara before and after modification were studied by scanning electron microscope and infrared spectroscopy. The results indicate that the adsorption process was more in line with the pseudo-second-order kinetic equation, and also in line with the Langmuir isotherm. The maximum adsorption capacity of OA and SOA for NR were 208.33 and 227.27 mg/g; 40.98 and 125.00 mg/g for MG, respectively. The regeneration efficiency of both adsorbents decreased after 5 cycles. The adsorption process is primarily governed by electrostatic attraction and hydrogen bonding between the adsorbent and the dye molecules (NR and MG). It is a multi-layer adsorption process and a spontaneous endothermic process.

Keywords: Adsorption isotherm; Biosorbent; Malachite green; Neutral red

1. Introduction

The global production of dyes amounts to 700,000 tons annually, with 10% of these dyes being discharged into the environment. Consequently, dyes have become one of the most detrimental pollutants present in industrial wastewater [1]. Even at low concentrations, dyes have a noticeable coloring effect on water [2]. This pollution not only detracts from the aesthetic appeal of natural surroundings but also poses significant risks to human health and the normal metabolic processes of aquatic organisms [3]. Malachite green (MG) finds extensive usage as a biocide in the worldwide aquaculture industry, where it is employed for the control of external fungal and protozoan infections in fish [4]. However, the permissible concentration of these dyes is exceedingly low, and elevated concentrations can exhibit toxicity towards aquatic animals. When ingested through the oesophagus, these substances give rise to carcinogenic, genotoxic, and chronic toxic effects within the human body [5]. Neutral red (NR) is often used as an indicator [6]. Its discharge into the water body is potentially harmful to the health of aquatic organisms, and it will also affect the sunlight penetration and gas solubility of the water body [7]. Collectively, these two dyes can inflict harm upon the water environment, severely disrupting its ecological equilibrium. In the event of their entry into the food chain, they may exert carcinogenic and mutagenic effects on human beings.

* Corresponding authors.

At present, the methods of treating dye wastewater are mainly divided into three categories: chemical method, biological method and physical method [8]. Chemical methods encompass various approaches such as electrochemical methods, photochemical methods, photocatalytic oxidation methods, ozone oxidation methods, and Fenton methods [9]. However, chemical methods are not economically appealing due to the need for specialized equipment, high energy consumption, substantial chemical reagent usage, and the production of toxic and detrimental secondary pollutants [10–13]. Biological method is a method that uses the metabolism of microorganisms to degrade pollutants and gradually convert organic matter in water into intermediate products or simple inorganic matter [14]. According to the types of microorganisms, biological methods can be divided into aerobic biological methods, anaerobic biological methods and aerobic–anaerobic combined methods [15]. However, the disadvantages of this method are the long processing time and the strict requirements for the processing environment. Among the three types of methods, the physical method emerges as the most suitable option, primarily encompassing adsorption, membrane separation, and magnetic separation [16]. While these physical methods may have minor limitations, they offer simplicity and high efficiency in comparison to the alternative approaches.

Adsorption method is defined as one of the most promising technologies because of its ability to efficiently separate various compound pollutants, and adsorption method has been widely used to remove various pollutants in water [17]. Due to the problem of adsorbent cost, scientists have focused on low-cost adsorbents [18]. For instance, certain researchers have explored the utilization of waste tea, converted into biochar and modified with polyethyleneimine, for the adsorption of activated black and methyl orange [19]. Other researchers use biochar made from persimmon peel to adsorb Methylene blue [20]. Biochar is a potential low-cost adsorbent that has attracted the interest of many researchers [21]. Notably, the adsorption of substances using biochar remains a relatively underexplored area of study. Agricultural wastes such as rice straw, rice husk, and bean dregs are widespread biomass. They have the characteristics of good porosity, large specific surface area (S_{BET}) and abundant functional groups (such as alcohols, aldehydes and other groups) with adsorption capacity [22]. Notably, these functional groups demonstrate a strong affinity for pollutants [23]. Some researchers use defatted algal biomass as an adsorbent to remove basic dyes from water [24], and *Eucalyptus angophoroides* bark as an adsorbent to remove dyes from water [25]. Although the adsorption performance of biomass may not rival that of commercial activated carbon, their potential remains immense.

Northeast China is one of the most important areas for soybean cultivation [26]. The processing of soybeans into edible products like soybean milk, tofu, and soy sauce results in the generation of substantial quantities of bean dregs, comprising cellulose, protein, carbohydrates, and other nutrients, which serve as the primary constituents of the investigated soybean residue biomass, referred to as okara adsorbent (OA) [27]. Notably, this cellulose-rich waste OA can be directly employed as an adsorbent for dye adsorption research [28]. Converting waste into adsorbents to absorb dyes is very beneficial to protect the environment [29]. Surfactants can improve the adsorption capacity of adsorbents. They usually contain both hydrophobic and hydrophilic groups, which help them adsorb various pollutants [30]. In this study, sodium dodecyl sulfate (SDS), an anionic surfactant, was utilized to modify the bean dregs adsorbent and investigate the adsorption efficiency of dyes, thereby resulting in the development of the modified adsorbent referred to as modified okara adsorbent (SOA).

This study focuses on investigating the adsorption behavior of NR and MG onto OA and SOA. Various parameters including contact time, pH, absorbent dosage, ionic strength, initial dye concentration, and temperature were examined. The adsorption kinetics and isotherms were analyzed, and a brief investigation into the adsorption mechanism was conducted. The primary objective of this research is to contribute to the removal of NR, MG, and other similar organic contaminants from the environment.

2. Materials and methods

2.1 Materials and reagents

Analytical pure NR and MG were purchased from M/s Tianjin Fuchen (Tianjin) Chemical Reagent Co., Ltd. SDS was purchased from M/s Sigma Corporation of the United States. OA was collected from M/s the Canteen of Northeast Agricultural University. Concentrated hydrochloric acid, absolute ethanol, and sodium bicarbonate were all analytical grades. Distilled water was used.

2.2. Characterization of materials

Before the adsorption experiment, OA and SOA were characterized and analyzed. For scanning electron microscopy (SEM), a small quantity of dry OA and SOA solid powder was uniformly applied to the sample stage. Any excess powder was removed using a rubber suction bulb, followed by a fine spray of gold powder for even distribution on the surface. The microporous structure of the material was studied using Brunauer–Emmett–Teller analysis (BET) (JW-BK112, China). Then, a scanning electron microscope (SU8010 M/s Hitachi, Tokyo, Japan) was used to observe and take pictures by selecting the appropriate magnification. The isoelectric point (pH_{PZC}) of OA and SOA were also measured. Add 0.01 mol/L NaCl solution to multiple 50 mL Erlenmeyer flasks, and adjust the pH value of the NaCl solution to 2.0–12.0 by adding 0.1 mol/L HCl or 0.1 mol/L NaOH range. Finally, 0.1 g of OA and SOA were added separately and shaken at 298 K for 48 h. After shaking, measure the final pH (pH_f) of the solution. To compare the changes in surface functional groups and chemical bonds before and after adsorption, the same tablets were prepared from the OA and SOA solid powders after dye adsorption for observation [31]. For X-ray diffraction (XRD), a small amount of dried OA and SOA solid powders were placed on a glass slide and observed by an X-ray diffractometer (D/Max 2200 M/s Rigaku Corporation, Japan). The experimental conditions are: Cu-Kα was used as the radiation source with a scanning range of 5°–70° and a scanning rate of 3°/min. For the Fourier-transform infrared spectroscopy (FTIR)

experiment, nominal quantities of desiccated solid powders of OA and SOA were admixed with potassium bromide (KBr) of exceptional purity. Subsequently, the resulting blends underwent mechanical milling, followed by compression into thin, uniform flakes. This sample preparation approach was executed to facilitate FTIR analysis. For FTIR measurements, we employed a Fourier-Transform Infrared Spectrometer (Model 8400S, Shimadzu Instruments Co., Ltd., Japan), a recognized instrument in the field. The spectra were acquired over a spectral region spanning from 4,000 to 400 cm^{-1}, a range typically suited for the elucidation of molecular structures and functional groups.

2.3. Preparation of adsorbents

A specified quantity of fresh soybean residue was taken and thoroughly washed with tap water and distilled water to eliminate larger impurity particles. Subsequently, the mixture was dried to a constant weight using an electric heating constant temperature blast drying oven set at 333 K, and then stored for future use. To remove any residual grease, the mixture underwent multiple washes using an organic solvent, ethanol, and a sodium bicarbonate solution. After each wash, it was dried to a constant weight. The dried mixture was then ground and passed through a 100-mesh sieve, resulting in the production of OA, which was carefully stored. For the modification of the cellulose absorbent, OA was soaked in a 0.00082 mol/L SDS solution, continuously stirred using a glass rod for 6 h. The material was then rinsed several times with distilled water to remove any excess reagents and subsequently dried to a constant weight in an electric heating constant temperature blast drying oven set at 333 K. After grinding, the SOA was obtained by passing it through a 100-mesh screen and stored for subsequent use.

2.4. Batch experiments

In this experiment, only one variable was altered to investigate its impact on the adsorption of OA and SOA. The variables manipulated included pH, contact time, initial dye concentration, Na^+ ion concentration, and temperature. Adjust the pH value of the solution in the range of 2.0–12.0 by adding 0.1 mol/L HCl or 0.1 mol/L NaOH. Since NR precipitates under alkaline conditions, pH values of 2.0, 3.0, 4.0, 5.0, and 6.0 were chosen to investigate the effect of pH of NR solution on the adsorption effect, whereas pH values of 2.0, 4.0, 6.0, 8.0, 10.0 and 12.0 were set to investigate the effect of pH of MG solution on the adsorption performance. Each group of experiments includes three parallel experiments and one control experiment. Five cycles of regenerative adsorption experiments were added to investigate its regeneration capacity and sustainability. Add 25 mL of NR or MG solution with a concentration of 25 mg/L and a certain amount of adsorbent in a 50 mL Erlenmeyer flask, and absorb for 2 h at a temperature of 298 K and an oscillation speed of 165 r/min. After that, the solution was filtered using a 0.45 mm syringe filter, the supernatant was centrifuged and placed in an ultraviolet spectrophotometer to measure the absorbance at 540 nm (for NR) and 616 nm (for MG). According to Lambert–Beer law, the standard curve method was used to calculate the concentration of NR and MG.

2.5. Adsorption kinetic and isotherm models

In this work, pseudo-first-order and pseudo-second-order model were used for adsorption kinetic analysis. Langmuir and Freundlich model were used to fit adsorption isotherms. The specific formula is as follows [32–34]:

$$\frac{1}{q_t} = \frac{1}{q_m} + \frac{t}{K_L q_m C_e} \tag{1}$$

$$R_L = \frac{1}{1 + K_L C_0} \tag{2}$$

$$\ln q_e = \frac{1}{n} \ln C_e + \ln K_F \tag{3}$$

$$\ln\left(q_e - q_t\right) = \ln\left(q_e\right) - k_1 t \tag{4}$$

$$\frac{t}{q_t} = \frac{1}{k_2 q_e^2} + \frac{t}{q_e} \tag{5}$$

where q_e is the adsorption amount at equilibrium, and q_t is the adsorption amount at time t. k_1 is the pseudo-first-order adsorption rate constant, and k_2 is the pseudo-second-order adsorption rate constant. K_L is the Langmuir equilibrium constant. R_L is the Langmuir separation factor. When the value is in the range of 0–1, the adsorption process is easy to proceed. C_e is the equilibrium concentration. K_F is the Freundlich constant, and it is related to the affinity of the adsorbent. The meaning of n value is the degree of influence of concentration on adsorption capacity. When $0 < 1/n < 1$, the adsorption process is easy. When $1/n > 1$, the adsorbent is not easy to proceed. It is a reliable way to use statistical physical models to examine and explain the adsorption mechanism related to pollutants. Two models were selected to simulate the unit adsorption of two dyes by OA and SOA.

3. Results and discussion

3.1. Characteristics of OA and SOA

The morphology of the adsorbent surface was observed by SEM, as shown in Fig. 1a and b. The surface of OA and SOA is irregular and rough with many folds, which may provide more sites for the dye. With BET, we measured S_{BET}, total hole volume, and average hole diameter. The S_{BET} of OA and SOA were 1.05 and 1.70 m^2/g, respectively, the total pore volume of OA and SOA were 0.0034 and 0.0056 mL/g, respectively, and the average hole diameter of OA and SOA is shown in Fig. 2a. From the XRD (Fig. 1c), the diffraction angle 2θ is about 22° and there is a main peak, which is the characteristic peak of cellulose, indicating the cellulose structure of OA and SOA. The pH_{PZC} is closely related to the electrostatic force between the adsorbents. When the $pH < pH_{PZC}$, the surface of the adsorbent is positively charged, which facilitates the adsorption of anions; otherwise, the surface of the adsorbent is negatively charged, which facilitates the adsorption of cations [35]. According to Fig. 1d, the pH_{PZC} of the OA is 5.50 and SOA is 5.70. Utilizing FTIR spectroscopy, one can discern the

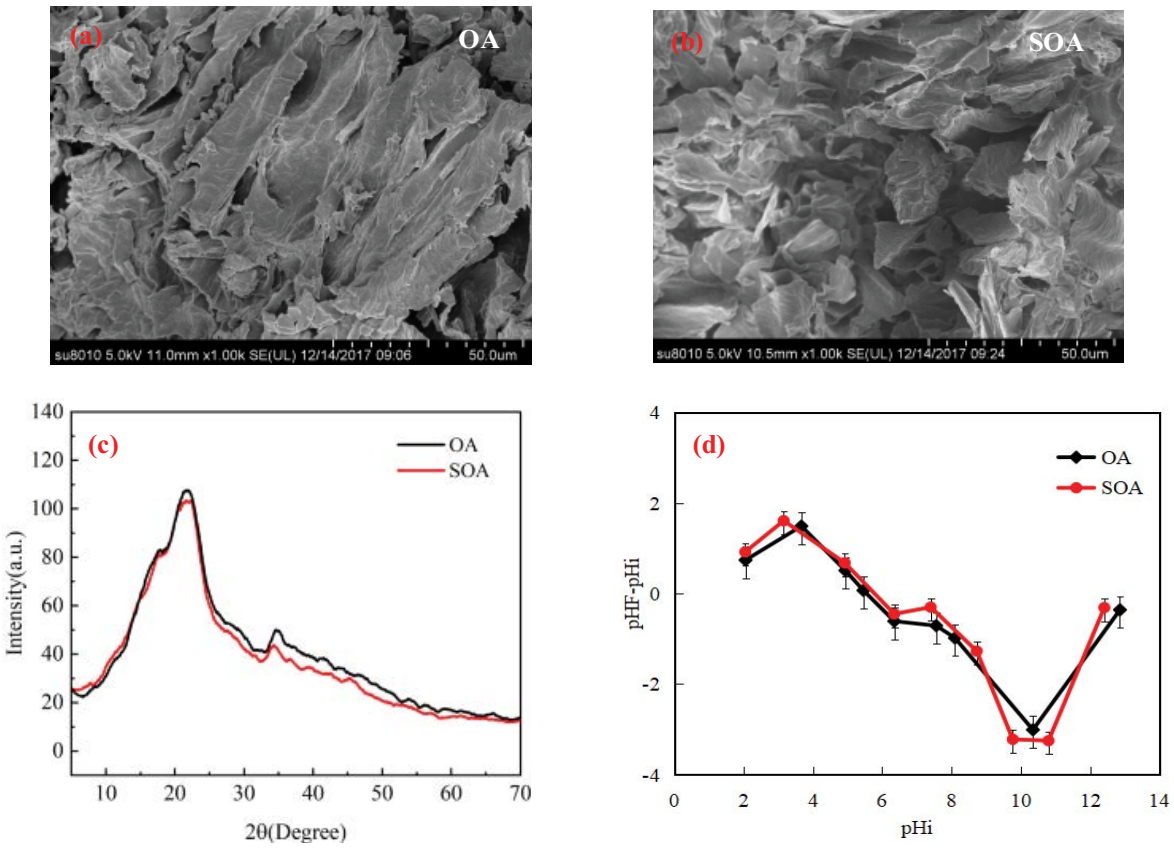

Fig. 1. Scanning electron microscopy image obtained for (a) OA, (b) SOA, (c) X-ray diffraction patterns obtained for OA and SOA, and (d) pH_{PZC} of OA and SOA.

distinctive functional groups within the adsorbent material. Moreover, a qualitative assessment of the pivotal functional groups can be deduced by contrasting infrared spectroscopy of the pristine and adsorbed materials. Fig. 3 presents the FTIR spectra of the OA and SOA adsorbents. At wavenumbers 3,434.77 and 2,926.21 cm^{-1}, conspicuous stretching vibrations corresponding to hydroxyl (O–H) and alkane (C–H) functionalities are evident, while at 1,053.92 cm^{-1}, a discernible peak associated with the ether bond (C–O–C) is apparent. These functional moieties represent characteristic constituents of cellulose, thus further corroborating the presence of cellulose components within the SD and MSD adsorbents. Additionally, vibrational modes attributed to carbonyl groups (C=O) in aldehydes and ketones are observable at 1,654.72 cm^{-1}. It is noteworthy that during the adsorption process of NR and MG, certain chemical bonds exhibit alterations in their peak positions, accompanied by the phenomenon known as "red-shifting". This phenomenon arises due to the superimposition of absorption peaks resulting from the stretching vibrations of specific chemical bonds. It indicates that charring of soya bean dregs at high temperature promotes the formation of aromatic groups [36]. Concurrently, some functional group absorption peaks demonstrate diminished sharpness, implying their active involvement in the adsorption process. Within this context, the most substantial variations in absorption peaks are observed for hydroxyl groups (O–H), carbonyl groups (C=O), and ether bonds (C–O–C). Therefore, it is reasonable to infer that these three functional groups may exert a pivotal influence on the adsorption process of NR and MG.

3.2. Effect of ionic strength

In this section, we investigate the effect of salt ion concentration in solution on the adsorption of dyes by OA and SOA. The concentration of salt ions in solution plays an important role in the adsorption process and can influence the overall efficiency of dye removal. By studying the effect of Na^+ concentrations from 0–0.5 mol/L, we can gain insight into the behaviour and performance of OA and SOA as adsorbents at different Na^+ levels. The results revealed that as the Na^+ concentration gradually increased within the range of 0–0.5 mol/L, both OA and SOA exhibited a gradual decrease in the removal efficiency of the two dyes. Specifically, for NR, the removal efficiency of OA decreased from 94.53% to 20.42%, while for MG, it decreased from 61.52% to 7.72%. Similarly, for SOA, the removal efficiency decreased from the initial values of 95.52% and 69.31% for NR and MG, respectively, to 20.04% and 7.72%. The observed decrease in the removal efficiency of OA and SOA can be attributed to the competition of Na^+ ions for active sites in the solution, resulting in reduced contact area between the adsorbent and the dyes. Consequently, the adsorption capacity of OA and SOA was weakened.

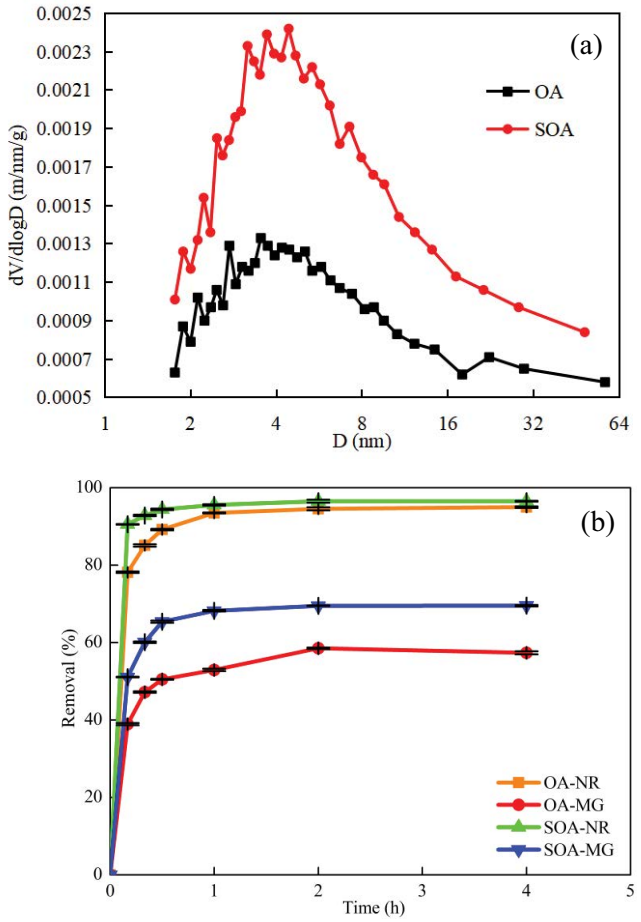

Fig. 2. Fourier-transform infrared spectra of the OA and SOA adsorbents.

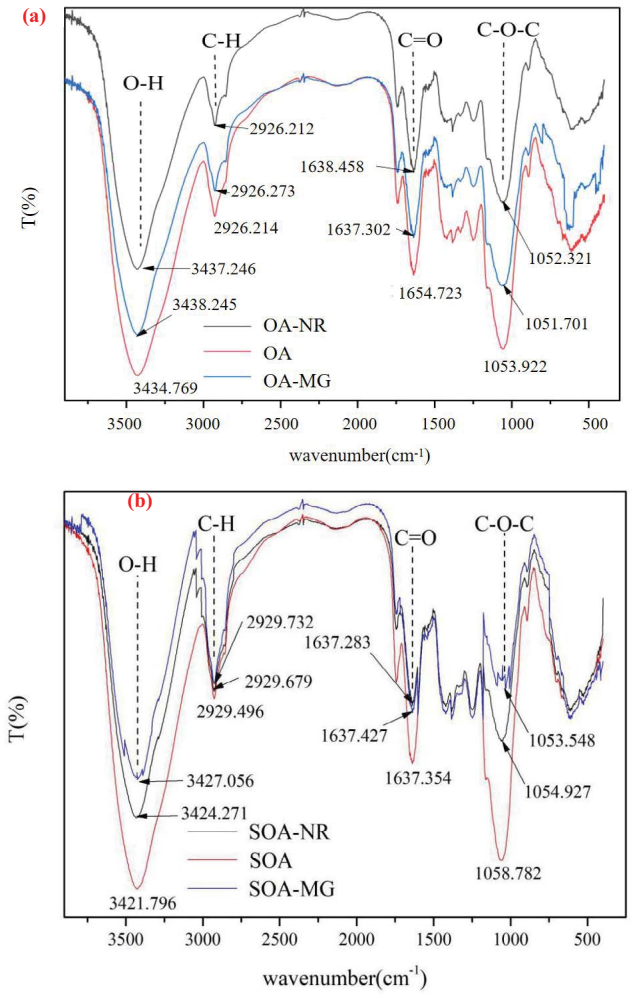

Fig. 3. Barrett–Joyner–Halenda method (desorption) differential integral pore volume and pore diameter logarithmic distribution curve.

3.3. Regenerative adsorption experimental

To further investigate the long-term stability and sustainability of the adsorbents, OA and SOA underwent 5 cycles of regeneration, as shown in Fig. 4. After 5 cycles, OA exhibited a decrease in regeneration efficiency for NR and MG, dropping from 94.35% and 96.52% to 69.69% and 71.37%, respectively. Similarly, SOA showed a similar trend with a decrease in regeneration efficiency for NR and MG, decreasing from 59.35% and 72.26% to 37.62% and 51.33%, respectively. This observed decline in regeneration efficiency may be attributed to the disruption of the original morphological structure caused by the ultrasonic treatment, which subsequently affects the adsorption performance.

3.4. Adsorption kinetics

Adsorption kinetics is an important indicator for studying the practicality of adsorbents. The adsorption rate curve depicted in Fig. 5a and b demonstrates that the adsorbent exhibits rapid adsorption initially, followed by a gradual approach towards equilibrium. To describe the kinetic adsorption data accurately, an appropriate adsorption kinetic model is employed. In this investigation, the pseudo-first-order and pseudo-second-order models were chosen for fitting purposes.

According to the data in Fig. 5 and Table 1, in the NR model fitting, the pseudo-second-order kinetic model has a very high degree of fitting to the adsorption process, and R^2 has reached 1.000. Comparing $q_{e,cal}$ with $q_{e,exp}$, it can be clearly seen that the fitting data obtained by the pseudo-second-order model is closer to the actual situation. Thus, the pseudo two-stage kinetic model, indicative of chemical adsorption, is deemed suitable for the entire adsorption process of OA and SOA [37]. At the same time, the k_1 and k_2 are both less than 1.000, indicating that the reaction rate is faster [38].

The fitting effect of the two dynamic models of MG is very good. The R^2 obtained by the fitting of the pseudo-first-order model is in the range of 0.9971–0.9976, while the R^2 obtained by the fitting of the pseudo-second-order model is in the range of 0.9957–0.9997. By comparing $q_{e,cal}$ and using the pseudo-second-order model to obtain data close to the value of $q_{e,exp}$, it is speculated that the adsorption process of MG is more in line with the pseudo-second-order model, and the main control of the adsorption process rate is chemical adsorption [39], k_2 is always less

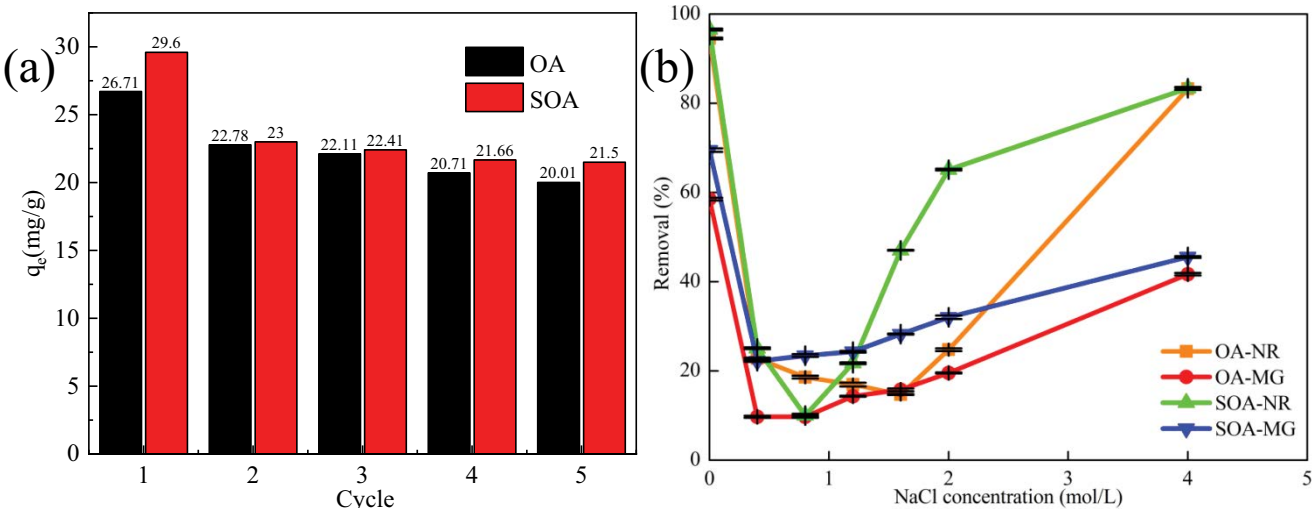

Fig. 4. Adsorption isotherm of OA and SOA, including Langmuir and Freundlich.

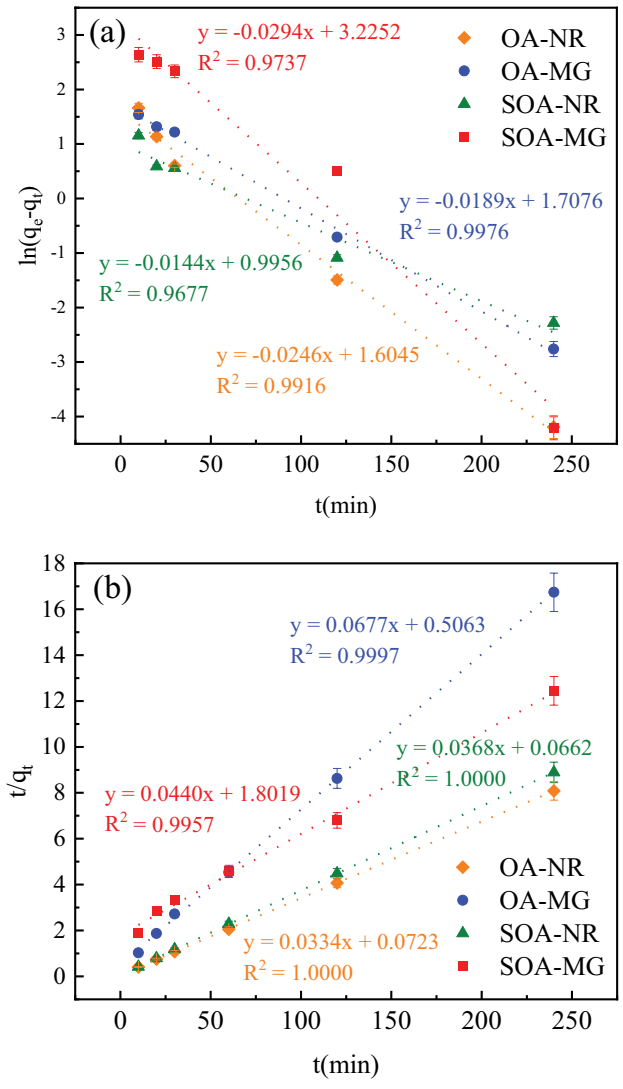

Fig. 5. Regeneration of OA and SOA through 5 cycles.

Table 1
Relative parameters table of kinetic models

Adsorbent	Models	Parameters	NR	MG
OA	Pseudo-first-order	k_1 (h^{-1})	0.0246	0.0189
		$q_{e,cal}$ (mg/g)	4.96	5.52
		R^2	0.9916	0.9976
	Pseudo-second-order	k_2 (g/mg·h)	0.015	0.090
		$q_{e,cal}$ (mg/g)	29.94	14.77
		R^2	1.000	0.9997
		$q_{e,exp}$ (mg/g)	29.70	14.40
SOA	Pseudo-first-order	k_1 (h^{-1})	0.0146	0.0212
		$q_{e,cal}$ (mg/g)	1.28	5.64
		R^2	0.9677	0.9737
	Pseudo-second-order	k_2 (g/mg·h)	0.060	0.010
		$q_{e,cal}$ (mg/g)	30.03	18.34
		R^2	1.000	0.9957
		$q_{e,exp}$ (mg/g)	30.00	18.10

than 1.000, indicating that the speed of this adsorption reaction is very fast [40].

3.5. Adsorption isotherm

Fig. 6 is the adsorption isotherm of NR and MG at 298 K, showing the relationship between the equilibrium concentration of the solution and the adsorption capacity. With the gradual increase of the concentration of the dye solution, the equilibrium adsorption capacity also increases, and the final curve tends to be stable. The maximum adsorption capacity (q_m) of OA and SOA for NR are 174.41 and 206.00 mg/g; 61.71 and 150.30 mg/g for MG. This can be explained by the fact that when the solution concentration is small, the adsorbent can provide enough adsorption sites. However, with a fixed amount of adsorbent added, as the solution concentration increases, the adsorption sites become

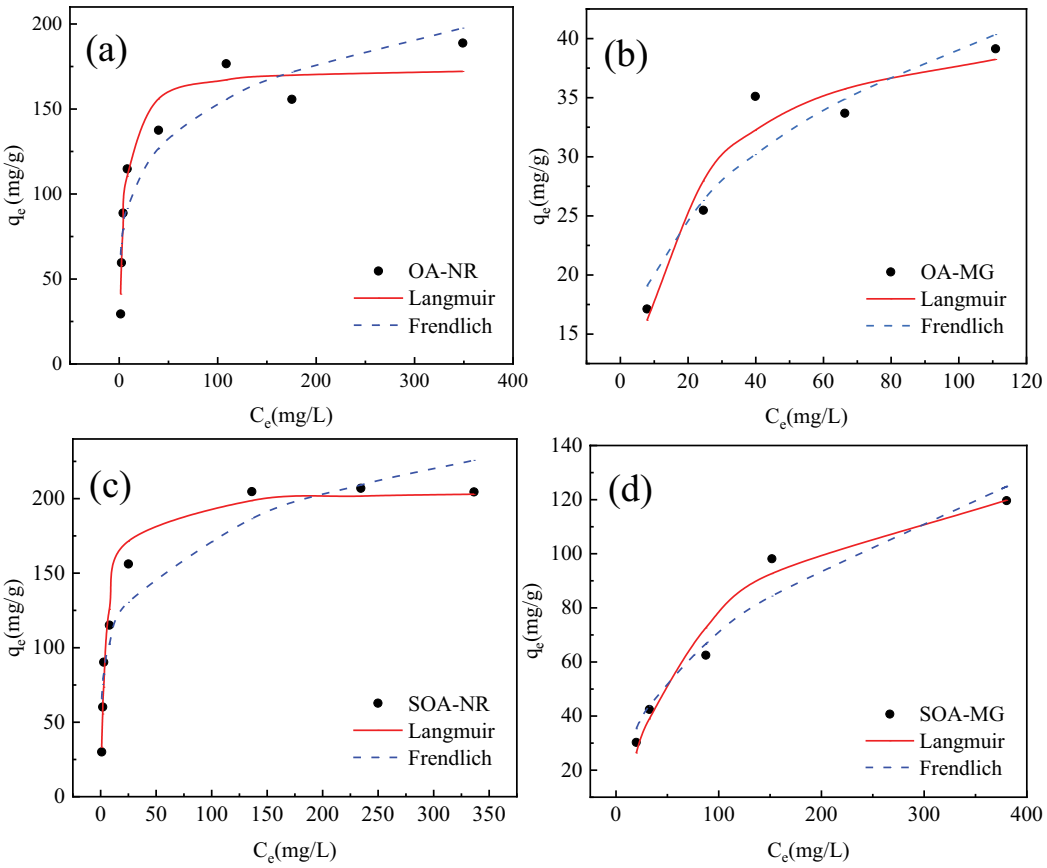

Fig. 6. Adsorption kinetics of OA and SOA (a) time and (b) pseudo-first-order and pseudo-second-order.

Table 2
Relative parameters of each fitting isotherm

Adsorbents	Dyes	Langmuir			Freundlich		
		q_m (mg/g)	K_L (L/mg)	R^2	K_F (L/mg)	n	R^2
OA	NR	174.41	0.21	0.9491	59.47	4.88	0.8733
	MG	42.69	0.08	0.9348	10.62	3.53	0.8987
SOA	NR	206.00	0.20	0.9793	66.12	4.74	0.9094
	MG	148.70	0.01	0.9731	8.82	2.24	0.9544

fully occupied, leading to a state of equilibrium where the adsorption capacity remains constant. In order to further explore the adsorption method, the above adsorption isotherm was fitted to the model. The adsorption isotherm models are: Langmuir and Freundlich isotherm model.

It can be seen from Table 2 that the adsorption process of NR is more in line with the Langmuir isotherm model. The R^2 values of OA and SOA are 0.9491 and 0.9793, respectively, which are much larger than the R^2 (0.8733 and 0.9094) obtained by the Freundlich isotherm model. This shows that the adsorption process is single-layer adsorption, and the surface of the adsorbent is uniform. At the same time, the q_m of NR of OA and SOA are 174.41 and 206.00 mg/g, respectively. These values are comparable to the experimental measurements, confirming a good fit with the Langmuir isotherm model. And through formula calculation, it is found that $R_L < 1.00$, indicating that the adsorption process is easy to proceed [41].

The R^2 values of the Langmuir isotherm model fitting process of OA and SOA adsorption of MG are 0.9348 and 0.9731, respectively, and the R^2 values of the Freundlich isotherm model fitting are 0.8987 and 0.9544, respectively. At the same time, the q_m, OA and SOA obtained from the Langmuir isotherm model are 42.69 and 148.70 mg/g, respectively. These results are similar to the value of the equilibrium adsorption capacity obtained in the actual adsorption isotherm. Therefore, the adsorption process of MG is more in-line with the Langmuir isotherm model. In addition, since the value of R_L is always less than 1.0, it can be understood that the adsorption process for MG is very simple [6,42]. In

general, the adsorption effects of NR on the above two dyes are better than that of MG. In order to show that both OA and SOA have better research prospects, this article lists the q_m of different adsorbents for different dyes, as shown in Table 3. Comparatively, the adsorbent employed in this study demonstrates enhanced adsorption efficacy compared to other adsorbents. For the adsorption of NR, OA and SOA have great potential and ability, while for MG, the adsorption effect of OA is moderate and that of SOA is excellent. In general, OA and SOA, as a cheap cellulose adsorbent, have low price and good adsorption effect, and have huge application potential.

3.6. Adsorption mechanisms

At present, existing studies show that common adsorption mechanisms include electrostatic interactions, π–π conjugates, hydrogen bonding, and intermolecular forces [43]. In this study, the adsorption mechanism was explored by analyzing the results of characterization measurements and adsorption experiments. The mechanism diagram is shown in Fig. 7. First, from the SEM image and S_{BET} measurement results, we can see that the surface of the adsorbent did not show obvious microporous structure instead, more folds provide adsorption sites [44]. Research indicates that

Table 3
Maximum adsorption of dyes by different adsorbent

Adsorbent	Dyes	q_m (mg/g)	References
Wheat straw	NR	25.47	[41]
Peanut husk	NR	37.50	[42]
Spent cottonseed hull substrate	NR	166.00	[43]
Biochar from crispy persimmon peel	NR	39.08	[44]
Charcoal T5	NR	30.21	[45]
OA	NR	208.33	This research
SOA		227.27	
Degreased coffee beans	MG	55.30	[46]
Brewers spent grain	MG	2.55	[47]
Chinese fan-falm biochar	MG	21.40	[48]
Sulfur-doped biochar derived from tapioca peel waste	MG	30.18	[49]
OA	MG	40.98	This research
SOA		125.00	

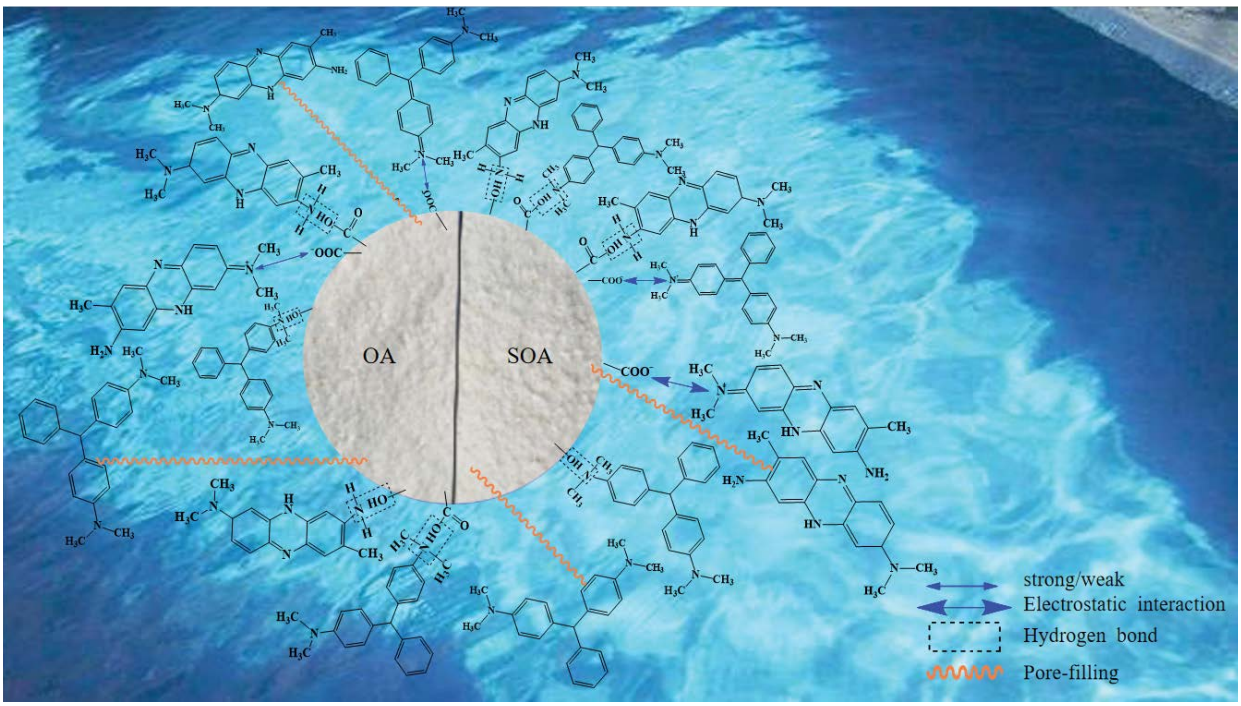

Fig. 7. Possible mechanism of OA and SOA removing Malachite green and Neutral red.

for organic molecules like dyes, the adsorption energy sites offered by edge folds favor adsorption, with minimal contribution from pore filling [45]. Subsequently, examination of the FTIR spectra of NR and MG adsorbed onto SOA revealed the abundance of oxygen-containing functional groups within the adsorbent, which possess negative charges. The combined action of these modes achieves the adsorption effect. Before and after adsorption, the functional groups that play a major role are hydroxyl (O–H) and carbonyl (C=O) for NR and the functional groups that play a major role are hydroxyl (O–H) for MG [46]. In the study, after modification with SOA, the surface of the SOA carried more anionic groups, which further enhanced the electrostatic attraction between the adsorbate and the adsorbent, which enhanced the adsorption effect and obtained the modification effect. At the same time, according to the influence of the pH of the solution on the experimental results, it can be predicted that the change in the pH of the solution has a very significant effect on the adsorption effect. From the side, it is explained that the electrostatic effect is the important role of the adsorbent SOA on the adsorbate. Some researchers used citric acid-modified soybean straw to adsorb copper ions in water [47]. By citric acid modification, the surface carries more –COOH groups. When the solution pH was 3.0, the group appears as the COO– form enhanced the electrostatic interaction with copper ions [48]. Consequently, the primary driving forces in the adsorption process between the adsorbent and NR and MG are electrostatic attraction and hydrogen bonding.

4. Conclusion

This study investigates the adsorption of two dyes, namely NR and MG, by OA and SOA, presenting a novel approach for treating dye wastewater. The modified material, SOA, exhibits superior performance compared to the unmodified material, OA, owing to the surface electronegativity enhancement achieved through SDS modification. The Langmuir model provides a better description of the dye adsorption process, with the maximum adsorption capacities (q_m) of OA and SOA for NR measured at 208.33 and 227.27 mg/g, respectively, and for MG at 40.98 and 125.00 mg/g, respectively. The pseudo-second-order kinetic model demonstrates good fitting, indicating that chemical adsorption governs the overall adsorption process. The regeneration efficiency of both OA and SOA decreased after 5 cycles. The analysis of adsorption and diffusion reveals that the diffusion model outside the membrane accurately describes the diffusion process, with external diffusion acting as the primary factor controlling the reaction rate. The interaction mechanism observed in the adsorption process involves electrostatic attraction, where adsorption occurs through the interaction between the cationic groups in the dye and the negatively charged functional groups on the adsorbent's surface. The adsorbent in this experiment was prepared by using a biomass material-bean dregs, with good adsorption effect, fast adsorption rate, low price and easy availability, simple preparation process and environmentally friendly, and it has application prospects as a new high-efficiency adsorbent.

Acknowledgements

This work was Supported by the Technological Project of Heilongjiang Province "the open competition mechanism to select the best candidates" (2022ZXJ05C02) and Research Program of Academic Backbone of Northeast Agricultural University. This work was Supported by the Program of Student Innovation Practice Training (SIPT) of Northeast Agricultural University (No. 202310224004).

References

[1] B.H. Beakou, K. El Hassani, M.A. Houssaini, M. Belbahloul, E. Oukani, A. Anouar, A novel biochar from *Manihot esculenta* Crantz waste: application for the removal of Malachite green from wastewater and optimization of the adsorption process, Water Sci. Technol., 76 (2017) 1447–1456.
[2] H. Jiang, Y.J. Dai, Vitamin C modified crayfish shells biochar efficiently remove tetracycline from water: a good medicine for water restoration, Chemosphere, 311 (2023) 136884, doi: 10.1016/j.chemosphere.2022.136884.
[3] W.H. Zou, H.J. Bai, S.P. Gao, Competitive adsorption of Neutral red and Cu^{2+} onto pyrolytic char: isotherm and kinetic study, J. Chem. Eng. Data, 57 (2012) 2792–2801.
[4] A. Mittal, Adsorption kinetics of removal of a toxic dye, Malachite green, from wastewater by using hen feathers, J. Hazard. Mater., 133 (2006) 196–202.
[5] H. Jiang, X. Li, J. Bai, W. Pan, Z. Luo, Y. Dai, Removal of ciprofloxacin lactate by phosphoric acid activated biochar: urgent consideration of new antibiotics for human health, Chem. Eng. Sci., 283 (2024) 119403, doi: 10.1016/j.ces.2023.119403.
[6] L.J. Zhang, D. Ma, G.Y. Mao, M.M. Zhang, R.P. Han, Adsorption of Neutral red from solution by bio-chars produced from pyrolysis of wheat straw, Adv. Mater. Res., 322 (2011) 72–76.
[7] J. Mittal, Permissible synthetic food dyes in India, Reson. – J. Sci. Educ., 25 (2020) 567–577.
[8] D.H.Y. Yanto, R.M. Chempaka, O.D. Nurhayat, B.D. Argo, T. Watanabe, Y. Wibisono, Y. Hung, Optimization of dye-contaminated wastewater treatment by fungal Mycelial-light expanded clay aggregate composite, Environ. Res., 231 (2023) 116207, doi: 10.1016/j.envres.2023.116207.
[9] J.H. Qu, Y. Xu, X.B. Zhang, M.Z. Sun, Y. Tao, X.M. Zhang, G.S. Zhang, C.J. Ge, Y. Zhang, Ball milling-assisted preparation of N-doped biochar loaded with ferrous sulfide as persulfate activator for phenol degradation: multiple active sites-triggered radical/non-radical mechanism, Appl. Catal., B, 316 (2022) 121639, doi: 10.1016/j.apcatb.2022.121639.
[10] X. Liu, Z.Y. Shao, Y.X. Wang, Y.F. Liu, S.Y. Wang, F. Gao, Y.J. Dai, New use for Lentinus edodes bran biochar for tetracycline removal, Environ. Res., 216 (2023) 114651, doi: 10.1016/j.envres.2022.114651.
[11] J. Wang, L.J. Qin, J.Y. Lin, J.Y. Zhu, Y.T. Zhang, J.D. Liu, B.V. der Bruggen, Enzymatic construction of antibacterial ultrathin membranes for dyes removal, Chem. Eng. J., 323 (2017) 56–63.
[12] W. Monika, Anion exchange resins as effective sorbents for acidic dye removal from aqueous solutions and wastewaters, Solvent Extr. Ion Exch., 30 (2012) 507–523.
[13] Y.J. Dai, Y.F. Liu, Y.L. Wang, W.Y. Fang, Y.M. Chen, Y.Y. Sui, A practice of conservation tillage in the mollisol region in Heilongjiang Province of China: a mini review, Pol. J. Environ. Stud., 32 (2023) 1479–1489.
[14] L. Liu, X.R. Wang, W.Y. Fang, X.H. Li, D.X. Shan, Y.J. Dai, Adsorption of metolachlor by a novel magnetic illite–biochar and recovery from soil, Environ. Res., 204 (2022) 111919, doi: 10.1016/j.envres.2021.111919.
[15] S. Ren, S. Wang, Y. Liu, Y. Wang, F. Gao, Y.J, Dai, A review on current pollution and removal methods of tetracycline in soil, Sep. Sci. Technol., 58 (2023) 2578–2602.
[16] J.H. Qu, Z.R. Li, F.X. Bi, X.B. Zhang, K.G. Li, M.Z. Sun, J. Ma, Y. Zhang, A multiple Kirkendall strategy for converting nanosized zero-valent iron to highly active Fenton-like

catalyst for organics degradation, Proc. Natl. Acad. Sci. U.S.A., 120 (2023) e2304552120, doi: 10.1073/pnas.2304552120.
[17] H. Jiang, X. Li, Y. Dai, Phosphoric acid activation of cow dung biochar for adsorbing enrofloxacin in water: icing on the cake, Environ. Pollut., 341 (2024) 122887.
[18] J.H. Qu, R. Liu, X. Bi, Z. Li, K. Li, Q. Hu, X. Zhang, G. Zhang, S. Ma, Y. Zhang, Remediation of atrazine contaminated soil by microwave activated persulfate system: performance, mechanism and DFT calculation, J. Cleaner Prod., 399 (2023) 136546, doi: 10.1016/j.jclepro.2023.136546.
[19] S. Wong, H.H. Tumari, N. Ngadi, N.B. Mohamed, O. Hassan, R. Mat, N.A.S. Amin, Adsorption of anionic dyes on spent tea leaves modified with polyethyleneimine (PEI-STL), J. Cleaner Prod., 206 (2019) 394–406.
[20] A. Ates, T. Oymak, Characterization of persimmon fruit peel and its biochar for removal of MB from aqueous solutions: thermodynamic, kinetic and isotherm studies, Int. J. Phytorem., 22 (2020) 607–616.
[21] J. Mittal, R. Ahmad, A. Mariyam, V.K. Gupta, A. Mittal, Expeditious and enhanced sequestration of heavy metal ions from aqueous environment by papaya peel carbon: a green and low-cost adsorbent, Desal. Water Treat., 210 (2021) 365–376.
[22] Y.J. Dai, J.J. Shi, N.X. Zhang, Z.L. Pan, C.M. Xing, X. Chen, Current research trends on microplastics pollution and impacts on agro-ecosystems: a short review, Sep. Sci. Technol., 57 (2022) 656–669.
[23] Z.G. Jia, Z.Y. Li, T. Ni, S.B. Li, Adsorption of low-cost absorption materials based on biomass (*Cortaderia selloana* flower spikes) for dye removal: kinetics, isotherms and thermodynamic studies, J. Mol. Liq., 229 (2017) 285–292.
[24] T.S. Chandra, S.N. Mudliar, S. Vidyashankar, S. Mukherji, R. Sarada, K. Krishnamurthi, V.S. Chauhan, Defatted algal biomass as a non-conventional low-cost adsorbent: surface characterization and MB adsorption characteristics, Bioresour. Technol., 184 (2015) 395–404.
[25] J.H. Qu, Q.J. Meng, W. Peng, J.J. Shi, Z.H. Dong, Z.R. Li, Q. Hu, G.S. Zhang, L. Wang, S.Y. Ma, Y. Zhang, Application of functionalized biochar for adsorption of organic pollutants from environmental media: synthesis strategies, removal mechanisms and outlook, J. Cleaner Prod., 423 (2023) 138690, doi: 10.1016/j.jclepro.2023.138690.
[26] W. Fu, X.Y. Zhang, J. Zhao, S.L. Du, R. Horton, M.T. Hou, Artificial warming-mediated soil freezing and thawing processes can regulate soybean production in Northeast China, Agric. For. Meteorol., 262 (2018) 249–257.
[27] B.Y.Z. Hiew, L.Y. Lee, X.J. Lee, S. Thangalazhy-Gopakumar, S.Y. Gan, Utilisation of environmentally friendly okara-based biosorbent for cadmium(II) removal, Environ. Sci. Pollut. Res., 28 (2021) 40608–40622.
[28] J.H. Qu, X.B. Zhang, S.Q. Liu, X.J. Li, S.Y. Wang, Z.H. Feng, Z.H. Wu, L. Wang, Z. Jiang, Y. Zhang, One-step preparation of Fe/N co-doped porous biochar for chromium(VI) and bisphenol a decontamination in water: insights to co-activation and adsorption mechanisms, Bioresour. Technol., 361 (2022) 127718, doi: 10.1016/j.biortech.2022.127718.
[29] C. Arora, P. Kumar, S. Soni, J. Mittal, B. Singh, Efficient removal of Malachite green dye from aqueous solution using *Curcuma caesia* based activated carbon, Desal. Water Treat., 195 (2020) 341–352.
[30] J. Shah, M.R. Jan, M. Zeeshan, M. Imran, Kinetic, equilibrium and thermodynamic studies for sorption of 2,4-dichlorophenol onto surfactant modified fuller's earth, Appl. Clay Sci., 143 (2017) 227–233.
[31] H. Li, X. Dong, S.E.B. Da L.M. Oliveira, Y. Chen, L.Q. Ma, Mechanisms of metal sorption by biochars: biochar characteristics and modifications, Chemosphere, 178 (2017) 466–478.
[32] K.Y. Foo, B.H. Hameed, Insights into the modeling of adsorption isotherm systems, Chem. Eng. J., 156 (2010) 2–10.
[33] K.L. Tan, B.H. Hameed, Insight into the adsorption kinetics models for the removal of contaminants from aqueous solutions, J. Taiwan Inst. Chem. Eng., 74 (2017) 25–48.
[34] M.E. González-López, C.M. Laureano-Anzaldo, A.A. Pérez-Fonseca, M. Arellano, J.R. Robledo-Ortíz, A critical overview of adsorption models linearization: methodological and statistical inconsistencies, Sep. Purif. Rev., 51 (2021) 358–372.
[35] A.H. Jawad, R.R. Abd, M.A.M. Ishak, L.D. Wilson, Adsorption of methylene blue onto activated carbon developed from biomass waste by H_2SO_4 activation: kinetic, equilibrium and thermodynamic studies, Desal. Water Treat., 57 (2016) 25194–25206.
[36] Q.F. Zheng, Y.H. Wang, Y.G. Sun, H.H. Niu, J.R. Zhou, Z.M. Wang, J. Zhao, FTIR study of the structural properties of biochar prepared from different materials and carbonisation methods, Spectrosc. Spectral Anal., 34 (2014) 962–966.
[37] Z. Reddad, C. Gerente, Y. Andres, P. Le Cloirec, Adsorption of several metal ions onto a low-cost biosorbent: kinetic and equilibrium studies, Environ. Sci. Technol., 36 (2002) 2067–2073.
[38] M.Z. Sun, J.H. Qu, T.Y. Han, J.Q. Xue, K.G. Li, Z. Jiang, G.S. Zhang, H. Yu, Y. Zhang, Resource utilization of bovine bone to prepare biochar as persulfate activator for phenol degradation, J. Cleaner Prod., 383 (2023) 135415, doi: 10.1016/j.jclepro.2022.135415.
[39] N. Ghasemi, M. Ghasemi, S. Moazeni, P. Ghasemi, N.S. Alharbi, V.K. Gupta, S. Agarwal, I.V. Burakova, A.G. Tkachev, Zn(II) removal by amino-functionalized magnetic nanoparticles: kinetics, isotherm, and thermodynamic aspects of adsorption, J. Ind. Eng. Chem., 62 (2018) 302–310.
[40] S.H. Ho, Y.D. Chen, Z.K. Yang, D. Nagarajan, J.S. Chang, N.Q. Ren, High-efficiency removal of lead from wastewater by biochar derived from anaerobic digestion sludge, Bioresour. Technol., 246 (2017) 142–149.
[41] S. Mohebali, D. Bastani, H. Shayesteh, Equilibrium, kinetic and thermodynamic studies of a low-cost biosorbent for the removal of Congo red dye: acid and CTAB-acid modified celery (*Apium graveo* lens), J. Mol. Struct., 1176 (2019) 181–193.
[42] H. Ma, J.B. Li, W.W. Liu, M. Miao, B.J. Cheng, S.W. Zhu, Novel synthesis of a versatile magnetic adsorbent derived from corncob for dye removal, Bioresour. Technol., 190 (2015) 13–20.
[43] W.Y. Qu, T. Yuan, G.J. Yin, S.A. Xu, Q. Zhang, H.J. Su, Effect of properties of activated carbon on Malachite green adsorption, Fuel, 249 (2019) 45–53.
[44] L.C. Dai, W.K. Zhu, L. He, F.R. Tan, N.M. Zhu, Q. Zhou, M.X. He, G.Q. Hu, Calcium-rich biochar from crab shell: an unexpected super adsorbent for dye removal, Bioresour. Technol., 267 (2018) 510–516.
[45] J. Wang, Z.M. Chen, B.L. Chen, Adsorption of polycyclic aromatic hydrocarbons by graphene and graphene oxide nanosheets, Environ. Sci. Technol., 48 (2014) 4817–4825.
[46] H.N. Tran, S.J. You, H.P. Chao, Insight into adsorption mechanism of cationic dye onto agricultural residues-derived hydrochars: negligible role of pi-pi interaction, Korean J. Chem. Eng., 34 (2017) 1708–1720.
[47] L.C. Dai, F.R. Tan, H. Li, N.M. Zhu, M.X. He, Q.L. Zhu, G.Q. Hu, L. Wang, J. Zhao, Calcium-rich biochar from the pyrolysis of crab shell for phosphorus removal, J. Environ. Manage., 198 (2017) 70–74.
[48] B. Zhu, T.X. Fan, D. Zhang, Adsorption of copper ions from aqueous solution by citric acid modified soybean straw, J. Hazard. Mater., 153 (2008) 300–308.